A hot and cold tumor-related prognostic signature for stage II colorectal cancer

MING ZHOU[1-4*], XIAOXU GE[1-4*], XIAOMING XU[5], BIAO SHENG[1-4], HAO WANG[1-4], HAOYU SHI[1-4], SIKUN LIU[1-4], BOREN TAN[1-4], KAILUN XU[6] and JIAN WANG[1-4]

[1]Department of Colorectal Surgery and Oncology, The Second Affiliated Hospital, Zhejiang University School of Medicine, Hangzhou, Zhejiang 310000, P.R. China; [2]Center for Medical Research and Innovation in Digestive System Tumors, Ministry of Education, Hangzhou, Zhejiang 310000, P.R. China; [3]Zhejiang Provincial Clinical Research Center for Cancer, Hangzhou, Zhejiang 310000, P.R China; [4]Cancer Center of Zhejiang University, Hangzhou, Zhejiang 310000, P.R. China; [5]Department of Pathology, The Second Affiliated Hospital, Zhejiang University School of Medicine, Hangzhou, Zhejiang 310000, P.R. China; [6]Department of Breast Surgery and Oncology, The Second Affiliated Hospital, Zhejiang University School of Medicine, Hangzhou, Zhejiang 310000, P.R. China

Received January 13, 2024; Accepted June 5, 2024

DOI: 10.3892/ol.2024.14552

Abstract. Globally, colorectal cancer (CRC) is one of the most lethal and prevalent malignancies. Based on the presence of immune cell infiltration in the tumor microenvironment, CRC can be divided into immunologically 'hot' or 'cold' tumors, which in turn leads to the differential efficacy of immunotherapy. However, the immune characteristics of hot and cold CRC tumors remain largely elusive, prompting further investigation of their properties regarding the tumor microenvironment. In the present study, a predictive model was developed based on the differential expression of proteins between cold and hot CRC tumors. First, the differentially expressed proteins (DEPs) were identified using digital spatial profiling and mass spectrometry-based proteomics analysis, and the pathway features of the DEPs were analyzed using functional enrichment analysis. A novel eight-gene signature prognostic risk model was developed (*IDO1*, *MAT1A*, *NPEPL1*, *NT5C*, *PTGR2*, *RPL29*, *TMEM126A* and *TUBB4B*), which was validated using data obtained from The Cancer Genome Atlas. The results revealed that the risk score of the eight-gene signature acted as an independent prognostic indicator in patients with stage II CRC (T3-4N0M0). It was also found that a high-risk score in the eight-gene signature was associated with high immune cell infiltration in patients with CRC. Taken together, these findings revealed some of the differential immune characteristics of hot and cold CRC tumors, and an eight-gene signature prognostic risk model was developed, which may serve as an independent prognostic indicator for patients with stage II CRC (T3-4N0M0).

Correspondence to: Dr Jian Wang, Department of Colorectal Surgery and Oncology, The Second Affiliated Hospital, Zhejiang University School of Medicine, 88 Jiefang Road, Shangcheng, Hangzhou, Zhejiang 310000, P.R. China
E-mail: wangjian519@zju.edu.cn

Dr Kailun Xu, Department of Breast Surgery and Oncology, The Second Affiliated Hospital, Zhejiang University School of Medicine, 88 Jiefang Road, Shangcheng, Hangzhou, Zhejiang 310000, P.R. China
E-mail: xukailun@zju.edu.cn

*Contributed equally

Key words: colorectal cancer, tumor microenvironment, prognosis, hot and cold tumor

Introduction

The composition and proportion of infiltrating immune cells varies across tumors, and may be associated with the specific biological properties of the tumor and its response to immunotherapy (1,2). Based on the characteristics of the tumor microenvironment (TME), tumors can be divided into 'cold' and 'hot' types (3,4). Hot tumors often exhibit immune cell infiltration and immune activation, whereas cold tumors exhibit significant features of low immune cell infiltration (4). At present, colorectal cancer (CRC) with high microsatellite instability is generally considered to be a hot tumor, and thus, patients may benefit from anti-PD-1/PD-L1 therapy (5-7). Conversely, microsatellite-stable (MSS) CRC exhibits profound heterogeneity regarding the immune ecosystem, and only a small percentage of patients are likely to benefit from immune-based combination therapy (8,9). Although there is an in-depth understanding of the molecular basis of CRC, the important contributing factors to the tumor immune microenvironment of CRC remain unclear (10). Therefore, further exploration is required to reveal the causes and characteristics of hot and cold colorectal tumors, which may be beneficial for the development of novel therapeutic strategies.

The infiltration of immune cells into tumors involves multiple processes and is influenced by intricate factors, such as tumor mutation burden (TMB), the presence of immune cells and the cytokines present (11,12). In general, tumors with

a higher TMB are considered to carry a higher neoantigen load that is essential for immune recognition and priming (13,14), whereas cold tumors are relatively incapable of initiating tumor immunity and being infiltrated due to a lower TMB and fewer neoantigens (15-18). Antigen-presenting cells (APCs) also serve a vital role in tumor immunity. Defects and alterations in tumor antigen processing and presentation machinery, such as the downregulated expression of the MHC-I molecule, limit antigen presentation in the face of tumor antigens (19-21). Dendritic cells, a type of APC, recruit T cells into the TME by secreting cytokines, such as CXCL10, the lack of which may lead to infiltration deficiency in cold tumors (22-24). Deficient T-cell homing to the tumor bed also accounts for immune infiltration deficiency in cold tumors (25). Previous studies have illustrated the association between the abnormal activation of the tumor cell-intrinsic oncogenic pathway and the absence of T-cell infiltration in melanoma (26) and CRC (27). The aberrant production and interactions of chemokines (28) and the extensive tumor vasculature (29) have been confirmed to increase T-cell infiltration in the tumor bed. In addition, immunosuppressive cells and cytokines can lead to T-cell exclusion from the tumor bed; for example, cancer-associated fibroblasts reduce T-cell responses and exert immunosuppressive effects through the production of the extracellular matrix, CXCL12, TGFβ and IL-6 (30-33).

Patients with CRC exhibit varying responses to different treatment regimens based on clinical stage. The prognosis of patients generally worsens as the cancer stage advances, particularly if the cancer is initially diagnosed at an advanced stage, with patients with early-stage CRC typically experiencing more favorable outcomes (34,35). For certain early-stage patients, there is no need for adjuvant chemotherapy and the intervals of postoperative follow-up surveillance can be adjusted appropriately. However, there are a few patients with early-stage CRC (stage I and stage II) that are at a high risk of recurrence and distant metastasis, resulting in a poorer prognosis, and this is related to the T stage, particularly T3 and T4 (36). Currently, prediction models for the prognosis of these patients with early-stage CRC are limited. In the present study, differential analyses were performed on hot and cold MSS CRC tumors using digital spatial profiling (DSP) and mass spectrometry (MS). Combined with CRC genomic expression profile data from The Cancer Genome Atlas (TCGA) database, a predictive risk model for the prognosis of early-stage CRC was developed, which may have potential guiding significance for treating early-stage CRC in the clinic.

Materials and methods

Patients. A total of 60 patients with MSS CRC, diagnosed between January 2010 and December 2012, were retrospectively enrolled in the present study. The clinicopathological data are shown in Table SI. The inclusion criteria were as follows: i) Patients who underwent surgical treatment at The Second Affiliated Hospital, Zhejiang University School of Medicine (Hangzhou, China), and were diagnosed with CRC by pathological, immunohistochemical and clinical examination; ii) patients with surgical specimens still available for paraffin sectioning; and iii) patients with complete case data and complete pathological data. The exclusion criteria were as follows: i) Patients suffering from primary tumors other than CRC or ii) patients undergoing primary lesion resection in an external hospital. The formalin-fixed paraffin-embedded (FFPE; fixed in 10% formalin at room temperature for 24-48 h) tissue sections (5 μm) were used for MS and DSP. Information on 378 patients with CRC with complete prognostic data was obtained from TCGA (https://cancergenome.nih.gov/; data were downloaded on July 27, 2023), and the entire cohort was randomly divided into the training cohort and the validation cohort at a ratio of 1:1 using R (version 4.3.0; https://www.r-project.org/) (Table SII).

MS-based proteomics. The proteomics data were obtained from our in-house CRC proteomics database. FFPE samples from patients were punched (weight range: 0.8-1.0 mg; diameter: 1.5 mm) using a Manual Tissue Arrayer MTA-1 (Beecher Instruments, Inc.), after which they were assessed to confirm that they contained both tumor tissue and stromal tissue with the guidance of hematoxylin and eosin (H&E) staining (10% hematoxylin staining for 5 min, 1% eosin solution staining for 2 min, at room temperature with a light microscope) by two senior pathologists. Pressure cycling technology coupled with data-independent acquisition (PCT-DIA) analysis of FFPE tissues was performed as described previously (37,38). Briefly, after dewaxing, rehydration and hydrolysis, FFPE tissues were digested using LysC and trypsin (Hualishi Tech. Ltd.) (39) with PCT assistance. Purified peptides were analyzed using an LTQ Orbitrap XL mass spectrometer (Thermo Q Exactive™ HF; Thermo Fisher Scientific, Inc.). DIA data were analyzed using DIA-NN software (version 1.7.4) (40).

DSP. Spatially resolved quantitation of 59 immunologically relevant proteins (including three normalization controls and three negative controls) were measured using the DSP platform (NanoString Technologies, Inc.; Table SIII). Previously prepared FFPE tissue microarray slides were stained with immunofluorescent antibodies to facilitate the identification of tissue morphology: Pan-cytokeratin (PanCK; 1:40; cat. no. NBP2-33200; Novus Biologicals, LLC; staining for 30 min at room temperature) for epithelial cells, CD45 (1:40; cat. no. NBP2-34528; Novus Biologicals, LLC; staining for 30 min at room temperature) for leukocytes, and SYTO13 (1:10; cat. no. S7575; Thermo Fisher Scientific, Inc.; staining for 15 min at room temperature) for nuclei. In each tissue core, at least one circular region of interest (ROI; measuring 300 μm in diameter) of cancerous tissue and one ROI of stromal tissue were selected. Upon exposure to ultraviolet light, the barcoded oligonucleotides corresponding to the 59 aforementioned antigen targets were released. They were collected via microcapillary aspiration and then dispensed into a 96-well plate. Digital counting was performed with the nCounter system (GeoMx DSP Control Center using the Data Analysis module V.2.4.0.421; NanoString, Inc.) and the data were normalized to internal controls.

Data processing. Only patients with CRC with adequate prognostic data were extracted from TCGA data. Log_2 transformation using R was used to process raw microarray data. The DSP and MS result data were standardized and de-batched using R.

Identification of hot and cold tumors. Tumor-infiltrating lymphocytes (TILs) of MSS CRC tumors were assessed by three senior pathologists using H&E-stained slides. A total of 60 patients were enrolled and divided into two groups: Cold CRC group (37 patients, TIL count ≤5%) and hot CRC group (23 patients, TIL count ≥20%).

Identification of DEPs between hot and cold tumors. The DEPs from the DSP cohorts and the MS cohorts between cold and hot tumors were analyzed using the Limma package (41) in R, and $P<0.05$ and $|\log_2\text{-fold change}|>0.5$ were set as the cutoff criteria.

Construction and validation of the prognostic model. Firstly, DEP IDs were converted into gene IDs to obtain differentially expressed genes (DEGs). Subsequently, the R package 'survival' (https://cran.r-project.org/web/packages/survival/index.html) was used to further construct the prognostic model. The prognostic value of each DEG was identified using univariate Cox regression analysis from R package. Next, LASSO regression analysis revealed potential risk genes and established an optimized polygenic risk score model. In the present study, bioinformatics software (X-Tile, 3.6.1) (42) was applied to identify the most optimal outcome-based cut-off value of the risk score. This method provides a graphical presentation of substantial subpopulations and presents the discovery of population cut-points based on biomarker expression. On the basis of this, the TCGA cohorts were divided into two groups (low-risk and high-risk groups). The performance and effectiveness of the model were assessed by Kaplan-Meier curve analysis and receiver operating characteristic (ROC) curve analysis. Furthermore, univariate and multivariate Cox regression analyses were performed with the risk scores as the independent variable. In addition, the clinicopathological features, including sex, age, pathological T stage, pathological N stage, pathological M stage and clinical stage, were divided into two groups, and Kaplan-Meier survival analysis was performed for each subgroup.

Establishment of a nomogram. The independence of the prognostic signature was assessed using univariate and multivariate Cox analyses in conjunction with clinical factors, including age and sex. The nomogram was established using the package 'rms' (https://hbiostat.org/r/rms/). Additionally, ROC curve analysis was performed to assess the prognostic value of the nomogram for predicting overall survival (OS).

Immune infiltration and immune checkpoint genes. The R package Estimation of STromal and Immune cells in MAlignant Tumor tissues using Expression data (ESTIMATE; https://bioinformatics.mdanderson.org/estimate/rpackage.html) was used to calculate the immune score, stromal score and ESTIMATE score between the high-risk group and the low-risk groups of patients with stage II CRC in the data obtained from TCGA. CIBERSORT (https://cibersortx.stanford.edu/) was used to calculate the proportions of immune cells. In addition, the relationships between the prognostic model and 15 important immune checkpoint genes were also studied using R.

Statistical analysis. SPSS Statistics version 22.0 (IBM Corp.) and R version 4.3.0 were used for statistical analysis. The Wilcoxon rank-sum test was used for comparison of two groups. Gene Ontology (GO) enrichment analysis and gene set enrichment analysis (GSEA) were performed using the R package clusterProfiler (https://bioconductor.org/packages/release/bioc/html/clusterProfiler.html) with a Fisher's exact test, and the P-values were adjusted using the Benjamini-Hochberg method. $^{*}P<0.05$ was considered to indicate a statistically significant difference.

Results

DSP and MS-based proteomics analysis for identification of DEPs between hot and cold MSS CRC tumors. A total of 60 patients were enrolled and divided into two groups: The cold CRC group (37 patients, TIL count ≤5%) and the hot CRC group (23 patients, TIL count ≥20%).

To evaluate the immune features of the TME, DSP analysis was performed on the 60 primary MSS CRC specimens. Based on the tumor (PanCK) and stroma (CD45) compartments, ROIs were identified (Fig. 1A). Comparing the hot CRC group with the cold CRC group: 20 upregulated proteins and one downregulated protein were identified (Fig. 1B; Table SIV).

Next, MS-based proteomics analysis was used to further identify DEPs between the two groups. As shown in Fig. 1C and Table SV, 57 proteins were upregulated and 191 proteins were downregulated in the hot CRC group compared with in the cold CRC group.

Functional enrichment analysis reveals the different functional pathways between hot and cold CRC. To gain a more comprehensive understanding of the functional significance of DEPs between the two groups, GO enrichment analysis was performed on the MS proteomics data. As shown in Fig. 2A, the upregulated proteins were primarily involved in biological processes, such as 'phagocytosis', 'myeloid leukocyte activation' and 'integrin-mediated signaling pathway'. To show more specific items in the biological processes, tree diagrams were employed, which revealed that most items were related to immune response (Fig. 2B). Neutrophil cytosol factor (NCF)1 was one of the most upregulated proteins that contributed to these biological processes (Fig. 2C), as well as NCF2 and NCF4, which belong to the NADPH oxidase complex. Additionally, integrin family members, including ITGAL, ITGAM and ITGB2, were upregulated and were involved in the aforementioned biological processes. Furthermore, GSEA revealed that the antigen processing and presentation pathway was prominently upregulated in hot CRC tissues (Fig. 2D).

The downregulated proteins were primarily involved in the various small molecule catabolic processes, such as 'organic acid catabolic process', 'carboxylic acid catabolic process' and 'monosaccharide metabolic process' (Fig. 2E and F). Enoyl coenzyme A hydratase domain-containing 2 and glutamate-pyruvate transaminase were the most significantly downregulated proteins of those involved in 'small molecule catabolic process' (Fig. 2G).

Construction and validation of a prognostic risk model of the eight-gene signature. The protein IDs of the DEPs

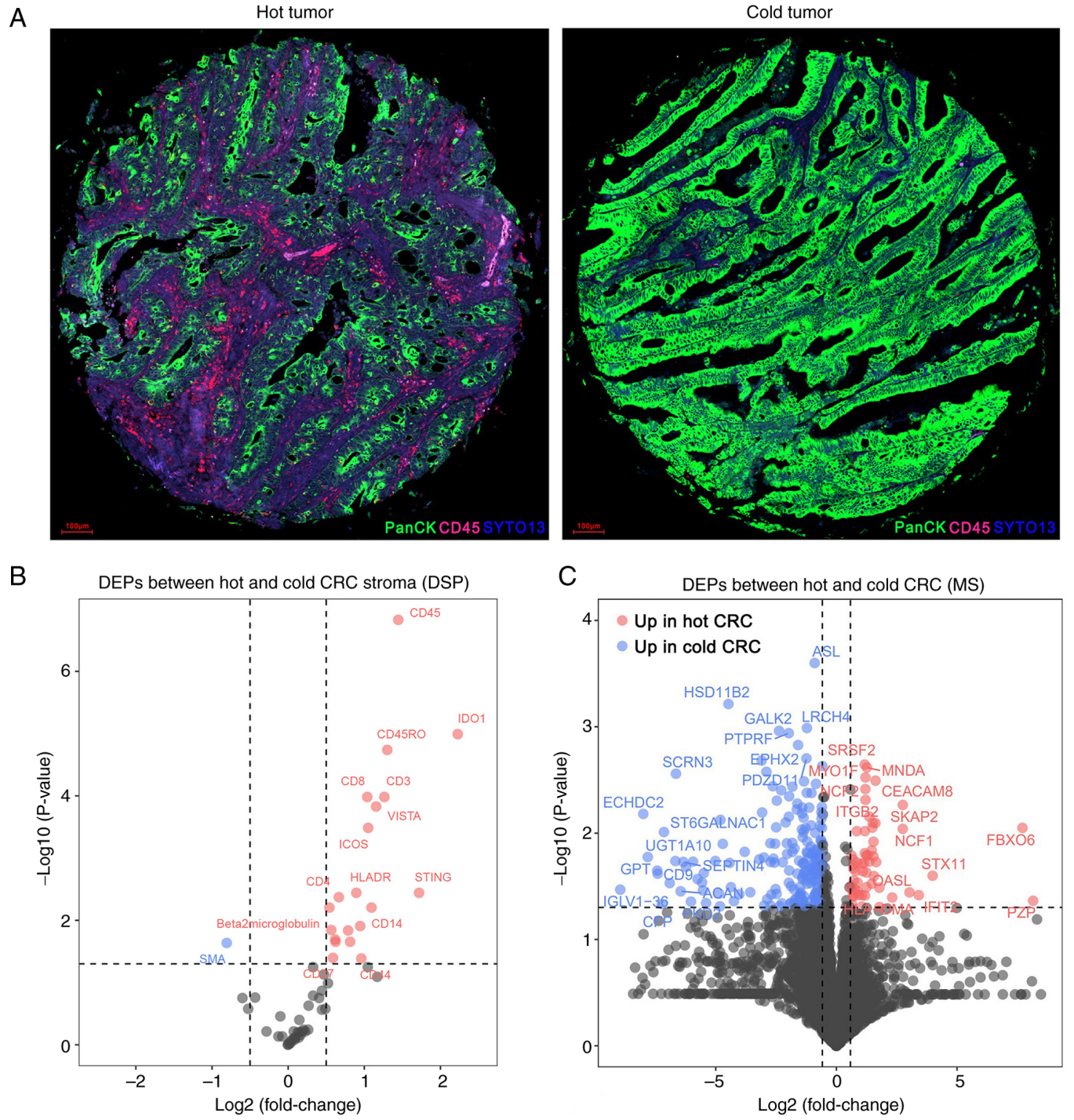

Figure 1. DSP- and MS-based proteomics analysis for the identification of DEPs between hot and cold CRC tumors. (A) Representative images of hot and cold tumors obtained by immunofluorescent staining for SYTO13 (blue), PanCK (green) and CD45 (red) using the NanoString DSP platform. SYTO13, PanCK and CD45 were used to characterize the nuclei, tumor and stroma compartments, respectively. (B) Volcano plot of the DEPs in the stroma compartment between primary hot and cold CRC tumor samples via DSP analysis. (C) Volcano plot of the DEPs between primary hot and cold CRC tumor samples via MS-based proteomics analysis. The vertical lines represent the $\log_2$ fold changes of -0.5 and 0.5, and the horizontal line represents the P-value of 0.05. DSP, digital spatial profiling; MS, mass spectrometry; CRC, colorectal cancer; DEP, differentially expressed protein.

obtained from differential analysis of the DSP- and MS-based proteomics data were converted into gene IDs. Notably, some protein IDs matched with multiple gene IDs and a total of 274 DEGs were identified (Table SVI). Univariate Cox regression analysis revealed that nine genes were markedly associated with prognosis in 189 patients from the data obtained from TCGA in the training cohort (Fig. 3A).

To guarantee the stability and viability of the clinical prognosis, eight genes (*IDO1*, *MAT1A*, *NPEPL1*, *NT5C*, *PTGR2*, *RPL29*, *TMEM126A* and *TUBB4B*) were identified after LASSO Cox analysis, which was used to further narrow the list of effective genes (Fig. 3B and C). Based on the products of mRNA expression levels and relative coefficients of each gene in the LASSO regression, the following

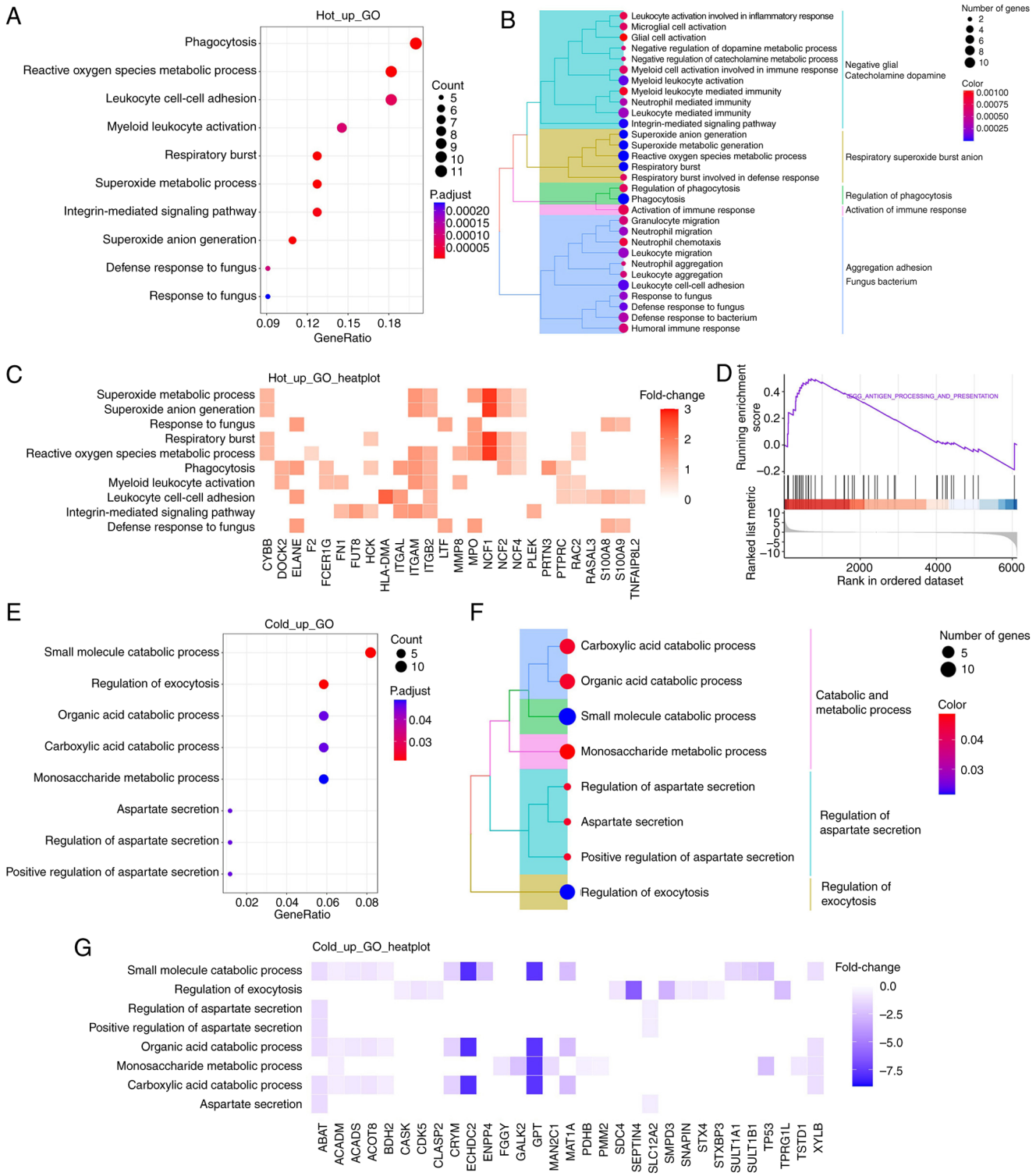

Figure 2. Functional enrichment analysis reveals the functional differential pathways between the hot and cold CRC tumors. (A) Bubble plots of the GO analysis of upregulated proteins in the hot CRC group. (B) Tree diagrams of the GO analysis of the upregulated proteins in the hot CRC group. Circle size, the number of genes contributing to the pathway. Color bar, adjusted P-value for the pathway. (C) Heatmap of the top ten biological processes and the expressions of the corresponding proteins. (D) Gene set enrichment analysis of antigen processing and presentation pathway genes. (E) Bubble plots of the GO analysis of downregulated proteins in the hot CRC group. (F) Tree diagrams of the GO analysis of the downregulated proteins in the hot CRC group. Circle size, the number of genes contributing to the pathway. Color bar, adjusted P value for the pathway. (G) Heatmap of the top eight biological processes and the expression of the corresponding proteins. CRC, colorectal cancer; GO, Gene Ontology.

predictive model was developed: Risk score=0.0968736 x *IDO1*-0.0445986 x *MAT1A*-0.0119460 x *NPEPL1*-0.0684733 x *NT5C*-0.1227449 x *PTGR2*-0.0994621 x *RPL29*-0.0026656 x *TMEM126A*-0.0018182 x *TUBB4B*.

To evaluate the validity of the prognostic model, the risk score, as determined by the eight-gene signature was calculated, and the most optimal cut-off value for the 189 patients in the training cohort from TCGA was identified with X-tile

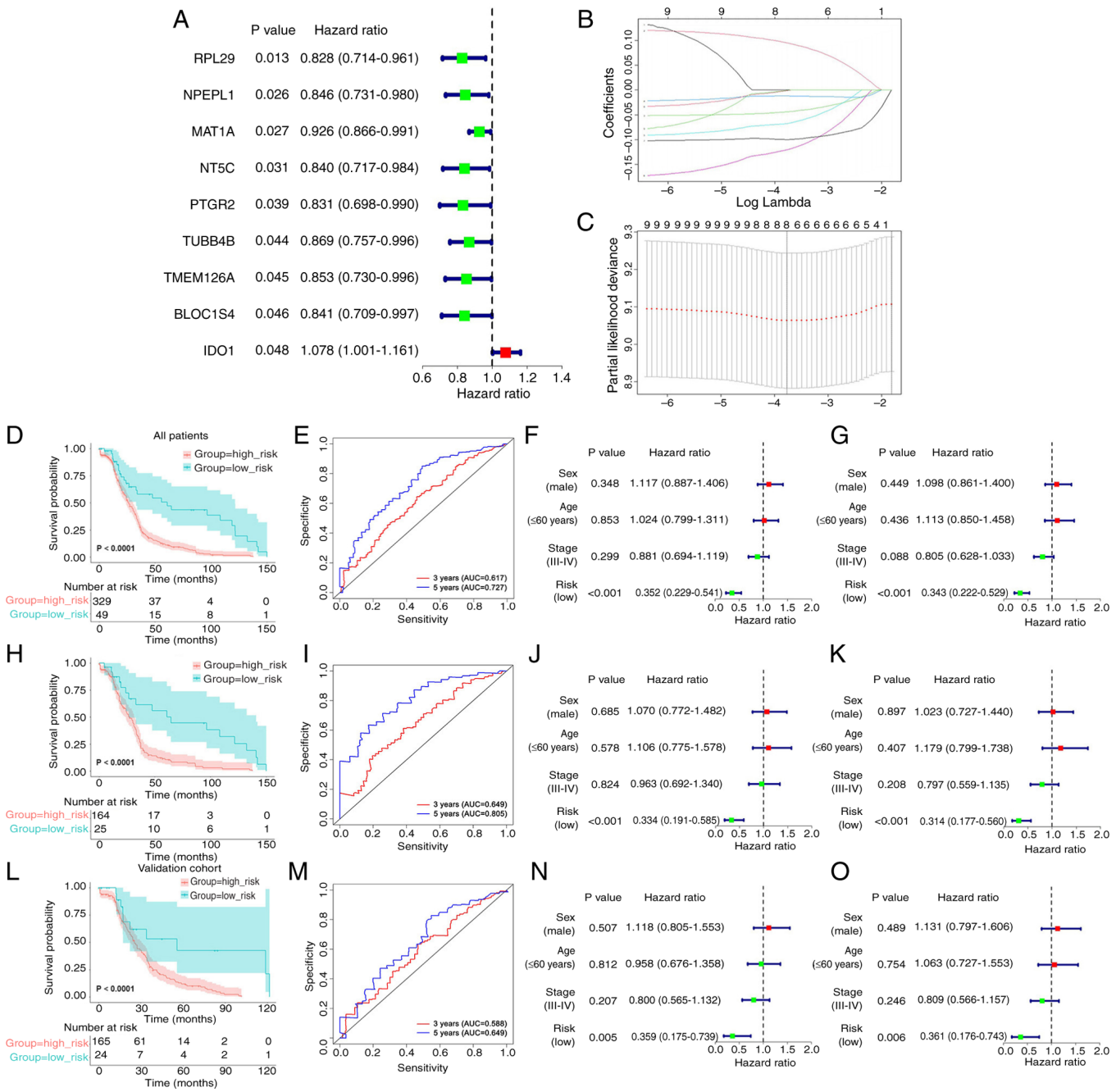

Figure 3. A prognostic risk model of the eight-gene signature constructed and validated using data obtained from TCGA. (A) Forest plot of the prognosis-related genes based on the univariate Cox regression analysis. (B) LASSO regression analysis was used to identify the eight-gene signature. (C) Cross-validation in the LASSO model. (D) Kaplan-Meier curve of the OS between the high- and low-risk subgroups in all patients from TCGA. (E) ROC curves of the eight-gene signature for 3- and 5-year OS in all patients from TCGA. Forest plots of the (F) univariate and (G) multivariate Cox regression analyses for the clinicopathological factors and the risk score in all patients from TCGA. (H) Kaplan-Meier curve of the OS between the high- and low-risk subgroups in the training cohort from TCGA. (I) ROC curves of the eight-gene signature for 3- and 5-year OS in the training cohort from TCGA. Forest plots of the (J) univariate and (K) multivariate Cox regression analyses for the clinicopathological factors and the risk score in the training cohort from TCGA. (L) Kaplan-Meier curve of the OS between the high- and low-risk subgroups in the validation cohort from TCGA. (M) ROC curves of the eight-gene signature for 3- and 5-year OS in the validation cohort from TCGA. Forest plots of the (N) univariate and (O) multivariate Cox regression analyses of the clinicopathologic factors and the risk score in the validation cohort from TCGA. TCGA, The Cancer Genome Atlas; OS, overall survival; AUC, area under the curve; ROC, receiver operating characteristic.

software. According to the most optimal cut-off value of the risk score (-2.70), the training cohort, the validation cohort and the full TCGA dataset were divided into low- and high-risk groups. Subsequently, through Kaplan-Meier analysis, it was noted that there was a difference between the two groups; the survival time was notably reduced in the high-risk score group (Fig. 3D, H and L). Moreover, the time-dependent ROC curves were plotted to verify that the prognostic model was accurate (Fig. 3E, I and M). Subsequently, the risk score was combined with other clinicopathological features, including sex, age and clinical stage, for the univariate (Fig. 3F, J and N) and multivariate (Fig. 3G, K and O) Cox analyses to explore

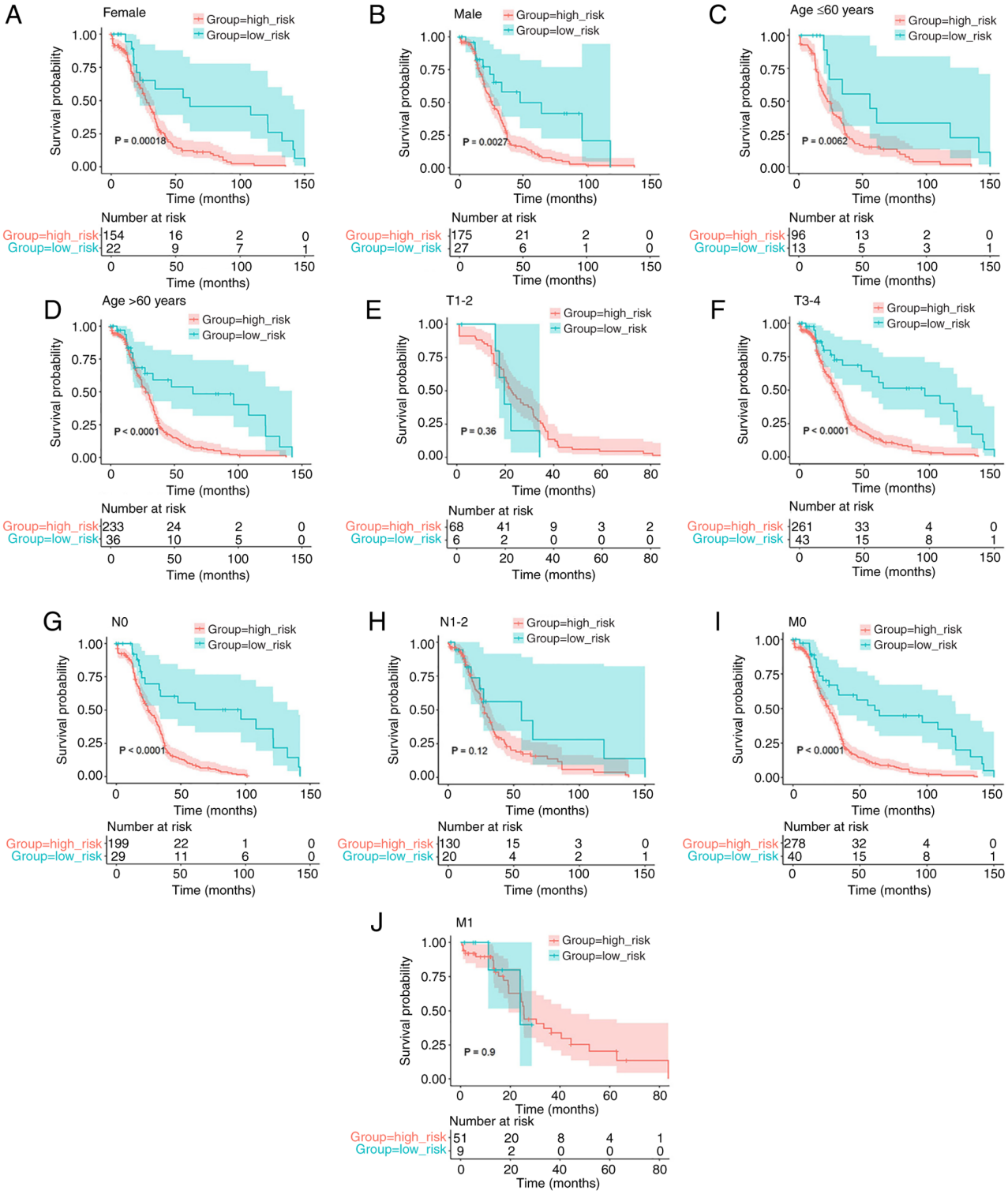

Figure 4. Kaplan-Meier analysis showing the association between the risk score of the eight-gene signature and survival in the different subgroups of patients. Kaplan-Meier curves showing the overall survival between the high- and low-risk subgroups in (A) female and (B) male patients, patients (C) aged ≤60 years and (D) aged >60 years old, and patients with stage (E) T1-2, (F) T3-4, (G) N0, (H) N1-2, (I) M0 and (J) M1 tumors.

its independence. Taken together, the results demonstrated that the risk score may be an independent prognostic factor.

Kaplan-Meier analysis shows an association between the risk score of the eight-gene signature and OS. To ensure that the prognostic model was accurate, Kaplan-Meier analysis was used to assess the predictive ability of the model stratified by sex, age (≤60 years or >60 years), pathological T stage (T1-2 or T3-4), pathological N stage (N0 or N1-2), and pathological M stage (M0 or M1) on the data obtained from TCGA. The survival analysis indicated an association between lower risk scores and improved OS rates in female (P=0.00018; Fig. 4A) and male (P=0.0027; Fig. 4B) patients, patients aged ≤60 years (P=0.0062; Fig. 4C) and >60 years (P<0.0001; Fig. 4D),

and patients with T3-4 (P<0.0001; Fig. 4F), N0 (P<0.0001; Fig. 4G) and M0 (P<0.0001; Fig. 4I) tumors. However, there was no association between the risk score of the eight-gene signature and prognosis in the T1-2 (P=0.36; Fig. 4E), N1-2 (P=0.12; Fig. 4H), and M1 (P=0.9; Fig. 4J) subgroups.

Risk score of the eight-gene signature serves as an independent prognostic indicator in patients with stage II CRC (T3-4N0M0). To further examine the effect of the risk score on the prognosis of different stages of CRC, Kaplan-Meier analysis was used to examine the association between the risk score and OS in the patients with stage I (T1-2N0M0), stage II (T3-4N0M0), stage III and stage IV CRC in the data obtained from TCGA. As shown in Fig. 5A-D, the results indicated that a high-risk score was associated with a poorer prognosis in patients with stage II (T3-4N0M0) CRC, but not in patients with stage I (T1-2N0M0), stage III or stage IV CRC. In addition, according to the AJCC 8th edition staging system of CRC (43), patients with M1 tumors (Fig. 4J) were classified as clinical stage IV (Fig. 5D).

By comparing the clinical characteristics, such as age and sex, univariate and multivariate Cox regression analyses were performed to investigate the independence of the prognostic model for patients with stage II CRC (T3-4N0M0) (Fig. 5E and F). The findings revealed that the risk score and age were highly significant prognostic indicators. To provide a more accurate prognosis for patients with stage II CRC (T3-4N0M0), a nomogram was established using the risk score and several clinicopathological factors, including age and sex. The concordance index of the nomogram was 0.612, which showed that the model was accurate in predicting the prognosis of patients with stage II CRC (T3-4N0M0) (Fig. 5G). The total score can be calculated using the score of each variable on the point scale of this nomogram and can be used to determine the probability of survival after 1-, 3- and 5-years. Furthermore, the predictive validity of the nomogram was assessed using ROC analysis. As shown in Fig. 5H, the areas under the curve for the prediction of 3- and 5-year OS were 0.661 and 0.782, respectively. Collectively, these results indicated that the risk score may serve as an independent prognostic indicator in patients with stage II CRC (T3-4N0M0).

Risk score is associated with the tumor immune infiltration characteristics in CRC. To determine the difference in immune infiltration between the high- and low-risk groups, the stromal, immune and ESTIMATE scores between the high- and low-risk groups in patients with stage II CRC were used. As shown in Fig. 6A, all three scores were significantly higher in the high-risk group than in the low-risk group (all P<0.001).

Next, the proportion of 22 types of immune cells between the high- and low-risk groups of patients with stage-II CRC was determined using CIBERSORT. According to the results, the proportion of macrophages (both M1 and M2) and resting mast cells were positively associated with the risk score, whereas the proportion of $CD4^+$ memory resting T cells and activated mast cells were negatively associated with the risk score (Fig. 6B).

Furthermore, the relationship between the risk score and the expression of 15 key immune checkpoint genes (*CD27*, *CD274*, *CD276*, *CD28*, *CD40*, *CTLA4*, *HAVCR2*, *ICOS*, *LAG3*, *PDCD1*, *TIGIT*, *TNFRSF18*, *TNFRSF4*, *TNFRSF9* and *VSIR*) was explored. The results illustrated that the expression of 12 immune checkpoint genes (*CD27*, *CD274*, *CD28*, *CTLA4*, *HAVCR2*, *ICOS*, *LAG3*, *PDCD1*, *TIGIT*, *TNFRSF18*, *TNFRSF4* and *TNFRSF9*) were elevated in the high-risk groups (Fig. 6C).

The relationships between the 15 key immune checkpoint genes and the eight selected genes in the prognostic model were next investigated. According to the median expression level of each gene, the cohort was divided into a high expression group and a low expression group of each gene. *PTGR2* exhibited positive associations with the expression of *CD28*, *CD40*, *ICOS* and *TIGIT* (Fig. 6D), whereas *RPL29* showed positive associations with the expression of *CD274*, *CD276*, *CD40*, *LAG3*, *PDCD1*, *TIGIT*, *TNFRSF9* and *VSIR* (Fig. 6E). As shown in Fig. 6F, *TMEM126A* exhibited positive associations with the expression of all the immune checkpoint genes, except *TNFRSF18*. *MAT1A* showed no relationship with any of the 15 immune checkpoint genes (Fig. 6G). *NPEPL1* was positively associated with the expression of *CD276*, *CD40*, *TNFRSF4* and *VSIR* (Fig. 6H). *NT5C* was positively associated with the expression of *CD276*, *CD40*, *LAG3*, *PDCD1*, *TNFRSF18*, *TNFRSF4* and *VSIR* (Fig. 6I). *TUBB4B* was positively associated with the expression of *CD274*, *CD276*, *CD40*, *LAG3*, *PDCD1*, *TIGIT*, *TNFRSF18*, *TNFRSF4* and *VSIR* (Fig. 6J). Finally, *IDO1* was positively correlated with the expression of all the immune checkpoint genes (Fig. 6K). These results demonstrated that differences in tumor immune infiltration were observed between the high- and low-risk groups, showing that a high-risk score may be associated with increased immune cell infiltration.

Discussion

Patients with CRC show differing levels of immune cell infiltration, and this is directly associated with the specific immunobiological behaviors of a tumor (44,45). The most fundamental reason for these differences is the tumor cells themselves. Thus, in the present study, patients with CRC were divided into hot and cold groups using immunofluorescent staining. Using MS, the differences in the expression of several proteins between hot and cold CRC tumors were examined and compared.

Compared with in cold CRC tumors, proteins that were upregulated in hot tumors were primarily enriched in immune-related pathways, including 'phagocytosis', 'leukocyte cell-cell adhesion', 'myeloid leukocyte activation' and 'integrin-mediated signaling pathway', amongst other processes. This result indicated that the immune interactions were relatively active in hot tumors. However, a large number of immune cells present in the TME do not attack the surrounding tumor cells. Therefore, a relative equilibrium state may be formed between cancer cells and tumor-infiltrating immune cells. According to the tumor stroma ROI DSP results, several vital immune-related proteins exhibited upregulated expression in hot CRC tumors, such as IDO1, STING, VISTA, PD-L1, 4-1BB and LAG3. The majority of these upregulated proteins are immune checkpoint molecules that may serve immunosuppressive functions to maintain a balance in immune tolerance status. Targeting these proteins may be a potential approach

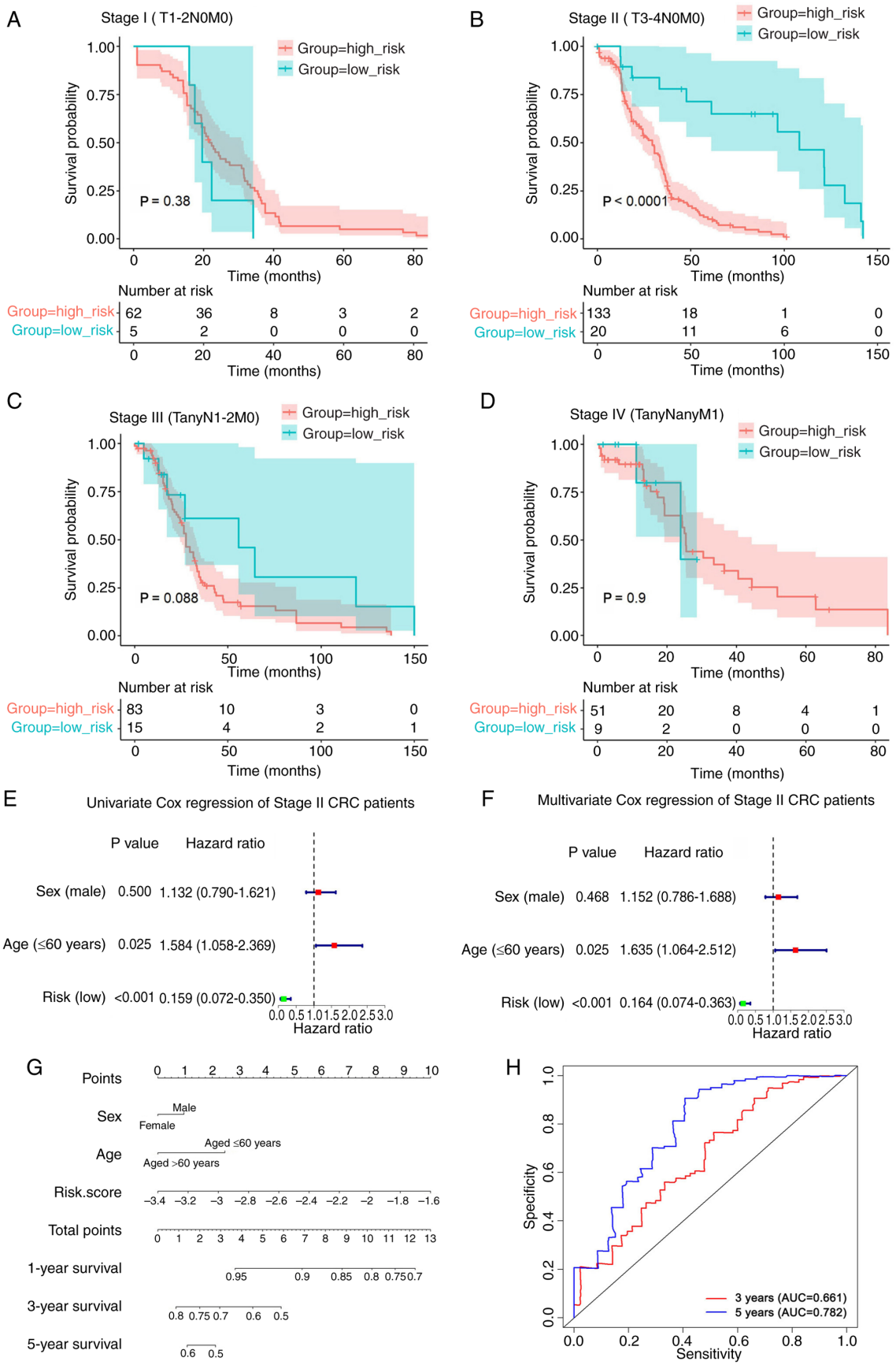

Figure 5. Risk score of the eight-gene signature serves as an independent prognostic indicator in patients with stage II CRC (T3-4N0M0). Kaplan-Meier curves for OS between the high- and low-risk subgroups in patients with (A) stage I (T1-2N0M0), (B) stage II (T3-4N0M0), (C) stage III and (D) stage IV CRC using data obtained from TCGA. Forest plots of (E) univariate and (F) multivariate Cox regression analyses for the clinicopathologic factors and the risk score in patients with stage II CRC (T3-4N0M0) using data obtained from TCGA. (G) Nomogram for predicting the 1-, 3- and 5-year OS in patients with stage II CRC (T3-4N0M0). (H) Receiver operating characteristic curves of the eight-gene signature for 3- and 5-year OS in patients with stage II CRC (T3-4N0M0). TCGA, The Cancer Genome Atlas; OS, overall survival; AUC, area under the curve; CRC, colorectal cancer.

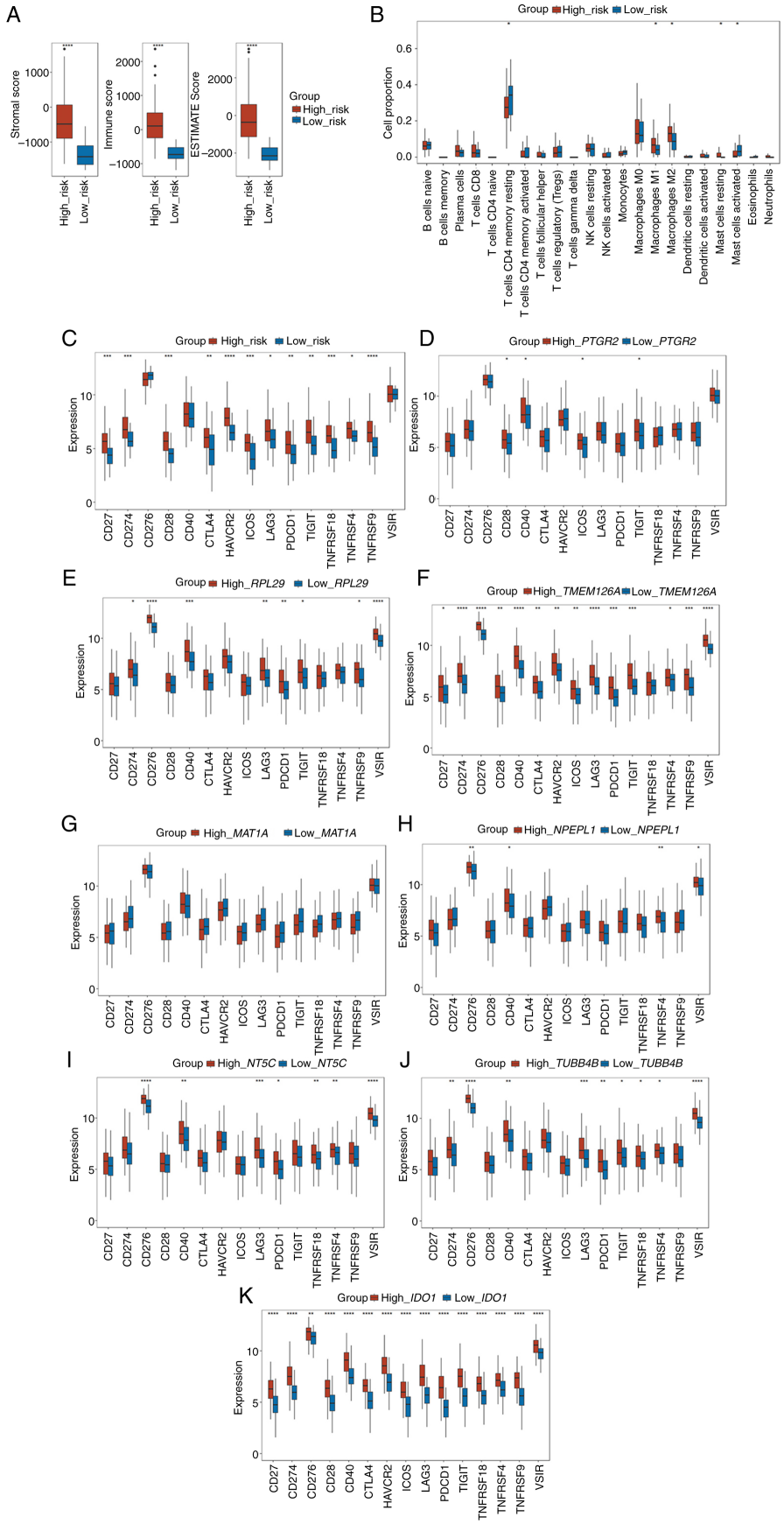

Figure 6. Risk score is associated with the tumor immune infiltration characteristics of colorectal cancer. (A) Box plots of the comparison of the stromal score, immune score, and ESTIMATE score between the high- and low-risk subgroups. (B) Box plots of the differences in the proportion of immune cells between the high- and low-risk subgroups. (C) Box plots of the differences in the expression of immune checkpoint genes between the high- and low-risk subgroups. Box plots of the differences in the expression of immune checkpoint genes between the high- and low-expression subgroups of (D) *PTGR2*, (E) *RPL29*, (F) *TMEM126A*, (G) *MAT1A*, (H) *NPEPL1*, (I) *NT5C*, (J) *TUBB4B* and (K) *IDO1*. *P<0.05, **P<0.01, ***P<0.001, ****P<0.0001. ESTIMATE, Estimation of STromal and Immune cells in MAlignant Tumor tissues using Expression data.

to disturb this balance and mobilize immune cells to attack tumor cells.

The protein expression profiles in cold colorectal tumors were distinct from those in the hot tumors. It was revealed that metabolism-related proteins were highly expressed in cold tumors, which may be related to the tumor metabolic microenvironment. These proteins may assist tumor cells in overcoming energy barriers and survive in a nutrient-deprived microenvironment. Moreover, the upregulated expression of SMA, a common marker of stromal cells (46), was observed in cold tumors. The stromal components of tumors are closely intertwined, and a barrier between tumor cells and immune cells is frequently formed (47). However, they do not directly contact each other, and the immune cells are not activated to attack tumor cells. Based on this, cold colorectal tumors with minimal immune cell infiltration exhibit limited sensitivity to immune monotherapy (48,49). Even though some effective treatments are available, such as chemotherapy or radiotherapy, which induce necrosis of tumor cells and antigen exposure, the immune cells and tumor antigens still do not directly contact the numerous stromal proteins. Therefore, the therapeutic efficacy of immunotherapy remains unsatisfactory.

Based on the MS and DSP differential expression analyses of hot and cold CRC tumors, a novel prognostic model was established. The model was validated using data from TCGA, and it was shown to perform well, whether in the training cohort, validation cohort or the overall TCGA CRC cohort. After subgroup analysis, it was demonstrated that this model had different predictive outcomes in different T stages, N stages and M stages. Compared with the T1-2 stage, the model showed higher predictive efficacy in patients with T3-4 stage tumors, which indicated that this model may be more appropriate for later T-stage patients, and this effect may be due to the fact that the model is based on comparisons between hot and cold tumors. The prognosis of patients with T1-2N0M0 CRC was relatively good and the tumor sizes were somewhat small. The DEGs between cold and hot CRC tumors had little effect on the differences in clinical outcomes of patients with T1-2N0M0 CRC. Conversely, the tumor sizes of patients with T3-4 stage CRC were likely larger. Thus, the infiltration of immune cells contributed more significantly to the biological behaviors of these tumors, and this model may have better predictive efficacy. In the N- and M-stage subgroup analysis, improved predictive efficacy was observed in the N0 or M0 subgroups. It is hypothesized that there are several risk factors for CRC prognosis. Lymph node metastasis or distant metastasis may exert a larger weighted effect; however, this model showed no significant differences between the N1-2 or M1 subgroups. Taking the aforementioned results together, it could be proposed that this model may have a better predictive effect on patients with stage II CRC (T3-4N0M0). It is worth mentioning that the treatment modalities of chemotherapy or radiation therapy are very complex, and the treatment information provided in TCGA database was limited. There might be numerous types of treatment, such as neoadjuvant chemotherapy, adjuvant chemotherapy, palliative chemotherapy or concurrent radiochemotherapy. Furthermore, the dosage, duration and timing of chemotherapy tended to vary between different patients, and the information was incomplete and ambiguous. Because of these confounding factors, the action of the risk score in assessing the predictive ability of the model stratified by therapy was not assessed.

Clinically, adjuvant chemotherapy is not routinely recommended for patients with stage II CRC as there is no evidence that adjuvant chemotherapy can improve survival for these patients. However, certain patients with stage II CRC may suffer from recurrence or distant metastasis, and thus have a poorer prognosis. At present, there are few prediction models for early-stage CRC. Li *et al* (50) reported that monosaccharide composites of circulating glycans in peripheral blood may serve as a diagnostic biomarker for early-stage detection of CRC. Additionally, based on gene expression profiles extracted from microarray datasets, immune-related or autophagy-related gene signatures were identified for the prognostic prediction of patients with early-stage CRC (51,52). However, the predictive model established in the present study differed from these previous models in terms of the sources of data. MS and DSP are both proteomics-based techniques used for detection and analysis. In almost every physiological process, proteins are the end products and functional molecules, and are thus more closely related to functional biological behaviors. In particular, the results of DSP show the protein expression levels in the stromal compartments, which is more accurate for the study of hot and cold tumors. Subsequently, data obtained from TCGA were used to construct and validate the prognostic model. Thus, the prognostic model developed was based on multi-omics data, and it should more accurately reflect the biological reality and is thus a more comprehensive prediction model.

Based on the results of the present study, patients with stage II CRC can be divided into high-risk and low-risk groups. Close monitoring is required for high-risk patients, and this may result in earlier detection of tumor recurrence and metastasis. Conversely, regular follow-up surveillance is sufficient for low-risk patients. This way, it is possible to treat patients with stage II CRC more accurately and in a more individualized manner.

Notably, it was revealed that the stromal score and immune score were markedly higher in the high-risk group of patients with stage II CRC, and these patients exhibited higher macrophage cell (both M1 and M2) and resting mast cell infiltrations, and lower $CD4^+$ memory resting T-cell and activated mast cell infiltrations in the tumors. The results demonstrated that the proportions of M1 and M2 macrophages were both positively associated with the risk score, and were both increased in the high-risk group. Therefore, it was hypothesized that there may be a significant difference in macrophage infiltration between these two groups. This requires more direct and sufficient evidence, and we aim to further investigate this aspect in future studies. The present study revealed higher expression levels of several immunosuppressive checkpoint genes in the high-risk group, including *HAVCR2*, *CD274*, *CTLA4*, *PDCD1*, *TIGIT* and *LAG3*. Meanwhile, certain immune-activating genes were also upregulated in the high-risk groups, such as *TNFRSF9*, *CD27* (*TNFRSF7*), *CD28*, *ICOS*, *TNFRSF18* and *TNFRSF4*. These may form a balance between immune suppression and activation. In addition, there was an association detected between the expression levels of certain genes in the risk score model and the expression of immune checkpoint genes. In particular, *IDO1*

and *TMEM126A* were positively associated with a number of immune checkpoint genes. All immune checkpoint genes were upregulated in the high-*IDO1* group, and most immune checkpoint genes, with the exception of *TNFRSF18*, were also upregulated in the high-*TMEM126A* group.

In conclusion, the model established in the present study is based on the differences in protein expression profiles between hot and cold CRC tumors. The primary objective of this model was to improve the prediction of patient prognosis. CRC tumors can be classified into two different immune types, which have various immune microenvironments, and carry a different risk of recurrence and metastasis. The proposed model had the best predictive outcomes on patients with stage II CRC, and may be used to guide the appropriate use of adjuvant chemotherapy and determine a suitable follow-up regime. As such, it provides important scientific value and carries potential clinical significance. Large-scale multicenter studies are required to confirm the applicability of the model for the prediction of efficacy. In the present study, a hot and cold tumor-related prognostic model for stage II colorectal cancer was mainly built. In the future, based on the results of the present study, we will select some genes from the present prognostic model for relevant functional validation and mechanism studies.

Acknowledgements

Not applicable.

Funding

This work was supported by the National Natural Science Foundation of China (grant no. 82072621) and the Zhejiang Medical and Health Science and Technology Plan Project (grant no. 2020KY688).

Availability of data and materials

The datasets analyzed in the present study may be found in TCGA database at the following URL: https://cancergenome.nih.gov/. The MS-based proteomics data generated in the present study were deposited in the National Genomics Data Center under accession number OMIX006709 or at the following URL: https://ngdc.cncb.ac.cn/omix/release/OMIX006709. The other data generated in the present study may be requested from the corresponding author.

Authors' contributions

MZ, XG, JW and KX designed and conceived the study. MZ, XG, JW, KX, XX, BS, HW, HS, SL and BT participated in data collection and wrote the manuscript. MZ and KX performed the data analysis and confirm the authenticity of all the raw data. JW and MZ contributed to the interpretation of the results and revised the manuscript. All authors have read and approved the final version of the manuscript.

Ethics approval and consent to participate

Human tissue samples were collected in this research; this retrospective study was conducted in accordance with the Declaration of Helsinki, and approved by the Institutional Ethics Committee of the Second Affiliated Hospital of Zhejiang University, School of Medicine (approval nos. 2020-0322 and 2021-0867). The patient consent for participation was waived due to the retrospective nature of the study.

Patient consent for publication

Not applicable.

Competing interests

The authors declare that they have no competing interests.

References

1. Paijens ST, Vledder A, de Bruyn M and Nijman HW: Tumor-infiltrating lymphocytes in the immunotherapy era. Cell Mol Immunol 18: 842-859, 2021.
2. Hanahan D and Coussens LM: Accessories to the crime: Functions of cells recruited to the tumor microenvironment. Cancer Cell 21: 309-322, 2012.
3. Kim TK, Vandsemb EN, Herbst RS and Chen L: Adaptive immune resistance at the tumour site: Mechanisms and therapeutic opportunities. Nat Rev Drug Discov 21: 529-540, 2022.
4. Duan Q, Zhang H, Zheng J and Zhang L: Turning cold into hot: Firing up the Tumor Microenvironment. Trends Cancer 6: 605-618, 2020.
5. Weng J, Li S, Zhu Z, Liu Q, Zhang R, Yang Y and Li X: Exploring immunotherapy in colorectal cancer. J Hematol Oncol 15: 95, 2022.
6. André T, Shiu KK, Kim TW, Jensen BV, Jensen LH, Punt C, Smith D, Garcia-Carbonero R, Benavides M, Gibbs P, *et al*: Pembrolizumab in Microsatellite-Instability-High advanced colorectal cancer. N Engl J Med 383: 2207-2218, 2020.
7. Casak SJ, Marcus L, Fashoyin-Aje L, Mushti SL, Cheng J, Shen YL, Pierce WF, Her L, Goldberg KB, Theoret MR, *et al*: FDA approval summary: Pembrolizumab for the First-line treatment of patients with MSI-H/dMMR advanced unresectable or metastatic colorectal carcinoma. Clin Cancer Res 27: 4680-4684, 2021.
8. Ganesh K: Optimizing immunotherapy for colorectal cancer. Nat Rev Gastroenterol Hepatol 19: 93-94, 2022.
9. Keum N and Giovannucci E: Global burden of colorectal cancer: Emerging trends, risk factors and prevention strategies. Nat Rev Gastroenterol Hepatol 16: 713-732, 2019.
10. Li J, Ma X, Chakravarti D, Shalapour S and DePinho RA: Genetic and biological hallmarks of colorectal cancer. Genes Dev 35: 787-820, 2021.
11. Zhang Y and Zhang Z: The history and advances in cancer immunotherapy: Understanding the characteristics of tumor-infiltrating immune cells and their therapeutic implications. Cell Mol Immunol 17: 807-821, 2020.
12. Kao KC, Vilbois S, Tsai CH and Ho PC: Metabolic communication in the tumour-immune microenvironment. Nat Cell Biol 24: 1574-1583, 2022.
13. Chan TA, Yarchoan M, Jaffee E, Swanton C, Quezada SA, Stenzinger A and Peters S: Development of tumor mutation burden as an immunotherapy biomarker: Utility for the oncology clinic. Ann Oncol 30: 44-56, 2019.
14. McGrail DJ, Pilié PG, Rashid NU, Voorwerk L, Slagter M, Kok M, Jonasch E, Khasraw M, Heimberger AB, Lim B, *et al*: High tumor mutation burden fails to predict immune checkpoint blockade response across all cancer types. Ann Oncol 32: 661-672, 2021.
15. Havel JJ, Chowell D and Chan TA: The evolving landscape of biomarkers for checkpoint inhibitor immunotherapy. Nat Rev Cancer 19: 133-150, 2019.
16. Zhang J, Huang D, Saw PE and Song E: Turning cold tumors hot: From molecular mechanisms to clinical applications. Trends Immunol 43: 523-545, 2022.
17. Galon J and Bruni D: Approaches to treat immune hot, altered and cold tumours with combination immunotherapies. Nat Rev Drug Discov 18: 197-218, 2019.
18. Westcott PMK, Sacks NJ, Schenkel JM, Ely ZA, Smith O, Hauck H, Jaeger AM, Zhang D, Backlund CM, Beytagh MC, *et al*: Low neoantigen expression and poor T-cell priming underlie early immune escape in colorectal cancer. Nat Cancer 2: 1071-1085, 2021.

19. Gettinger S, Choi J, Hastings K, Truini A, Datar I, Sowell R, Wurtz A, Dong W, Cai G, Melnick MA, *et al*: Impaired HLA class I antigen processing and presentation as a mechanism of acquired resistance to immune checkpoint inhibitors in lung cancer. Cancer Discov 7: 1420-1435, 2017.
20. Yamamoto K, Venida A, Yano J, Biancur DE, Kakiuchi M, Gupta S, Sohn ASW, Mukhopadhyay S, Lin EY, Parker SJ, *et al*: Autophagy promotes immune evasion of pancreatic cancer by degrading MHC-I. Nature 581: 100-105, 2020.
21. Burr ML, Sparbier CE, Chan KL, Chan YC, Kersbergen A, Lam EYN, Azidis-Yates E, Vassiliadis D, Bell CC, Gilan O, *et al*: An Evolutionarily conserved function of polycomb silences the MHC class I antigen presentation pathway and enables immune evasion in cancer. Cancer cell 36: 385-401.e8, 2019.
22. Spranger S, Dai D, Horton B and Gajewski TF: Tumor-residing batf3 dendritic cells are required for effector T cell trafficking and adoptive T cell therapy. Cancer Cell 31: 711-723.e4, 2017.
23. Wculek SK, Cueto FJ, Mujal AM, Melero I, Krummel MF and Sancho D: Dendritic cells in cancer immunology and immunotherapy. Nat Rev Immunol 20: 7-24, 2020.
24. Hegde S, Krisnawan VE, Herzog BH, Zuo C, Breden MA, Knolhoff BL, Hogg GD, Tang JP, Baer JM, Mpoy C, *et al*: Dendritic cell paucity leads to dysfunctional immune surveillance in pancreatic cancer. Cancer Cell 37: 289-307.e9, 2020.
25. Liu YT and Sun ZJ: Turning cold tumors into hot tumors by improving T-cell infiltration. Theranostics 11: 5365-5386, 2021.
26. Spranger S, Bao R and Gajewski TF: Melanoma-intrinsic β-catenin signalling prevents anti-tumour immunity. Nature 523: 231-235, 2015.
27. Grasso CS, Giannakis M, Wells DK, Hamada T, Mu XJ, Quist M, Nowak JA, Nishihara R, Qian ZR, Inamura K, *et al*: Genetic mechanisms of immune evasion in colorectal cancer. Cancer Discov 8: 730-749, 2018.
28. Dangaj D, Bruand M, Grimm AJ, Ronet C, Barras D, Duttagupta PA, Lanitis E, Duraiswamy J, Tanyi JL, Benencia F, *et al*: Cooperation between constitutive and inducible chemokines enables T cell engraftment and immune attack in solid tumors. Cancer Cell 35: 885-900.e10, 2019.
29. Apte RS, Chen DS and Ferrara N: VEGF in signaling and disease: Beyond discovery and development. Cell 176: 1248-1264, 2019.
30. Feig C, Jones JO, Kraman M, Wells RJ, Deonarine A, Chan DS, Connell CM, Roberts EW, Zhao Q, Caballero OL, *et al*: Targeting CXCL12 from FAP-expressing carcinoma-associated fibroblasts synergizes with anti-PD-L1 immunotherapy in pancreatic cancer. Proc Natl Acad Sci USA 110: 20212-20217, 2013.
31. Sahai E, Astsaturov I, Cukierman E, DeNardo DG, Egeblad M, Evans RM, Fearon D, Greten FR, Hingorani SR, Hunter T, *et al*: A framework for advancing our understanding of cancer-associated fibroblasts. Nat Rev Cancer 20: 174-186, 2020.
32. McAndrews KM, Chen Y, Darpolor JK, Zheng X, Yang S, Carstens JL, Li B, Wang H, Miyake T, Correa de Sampaio P, *et al*: Identification of functional heterogeneity of Carcinoma-Associated fibroblasts with distinct IL6-Mediated therapy resistance in pancreatic cancer. Cancer Discov 12: 1580-1597, 2022.
33. de Visser KE and Joyce JA: The evolving tumor microenvironment: From cancer initiation to metastatic outgrowth. Cancer Cell 41: 374-403, 2023.
34. Tang J, Yan T, Bao Y, Shen C, Yu C, Zhu X, Tian X, Guo F, Liang Q, Liu Q, *et al*: LncRNA GLCC1 promotes colorectal carcinogenesis and glucose metabolism by stabilizing c-Myc. Nat Commun 10: 3499, 2019.
35. Dekker E, Tanis PJ, Vleugels JLA, Kasi PM and Wallace MB: Colorectal cancer. Lancet 394: 1467-1480, 2019.
36. Li J, Guo BC, Sun LR, Wang JW, Fu XH, Zhang SZ, Poston G and Ding KF: TNM staging of colorectal cancer should be reconsidered by T stage weighting. World J Gastroenterol 20: 5104-5112, 2014.
37. Guo T, Kouvonen P, Koh CC, Gillet LC, Wolski WE, Röst HL, Rosenberger G, Collins BC, Blum LC, Gillessen S, *et al*: Rapid mass spectrometric conversion of tissue biopsy samples into permanent quantitative digital proteome maps. Nat Med 21: 407-413, 2015.
38. Cai X, Xue Z, Wu C, Sun R, Qian L, Yue L, Ge W, Yi X, Liu W, Chen C, *et al*: High-throughput proteomic sample preparation using pressure cycling technology. Nat Protoc 17: 2307-2325, 2022.
39. Sun Y, Selvarajan S, Zang Z, Liu W, Zhu Y, Zhang H, Chen W, Chen H, Li L, Cai X, *et al*: Artificial intelligence defines protein-based classification of thyroid nodules. Cell Discov 8: 85, 2022.
40. Demichev V, Messner CB, Vernardis SI, Lilley KS and Ralser M: DIA-NN: Neural networks and interference correction enable deep proteome coverage in high throughput. Nat Methods 17: 41-44, 2020.
41. Ritchie ME, Phipson B, Wu D, Hu Y, Law CW, Shi W and Smyth GK: Limma powers differential expression analyses for RNA-sequencing and microarray studies. Nucleic Acids Res 43: e47, 2015.
42. Camp RL, Dolled-Filhart M and Rimm DL: X-tile: A new bio-informatics tool for biomarker assessment and outcome-based cut-point optimization. Clin Cancer Res 10: 7252-7259, 2004.
43. Amin MB, Edge SB, Greene FL, Byrd DR, Brookland RK, Washington MK, Gershenwald JE, Compton CC, Hess KR, Sullivan DC, *et al*: AJCC Cancer Staging Manual. Springer International Publishing, New York, NY, 2017.
44. Bruni D, Angell HK and Galon J: The immune contexture and Immunoscore in cancer prognosis and therapeutic efficacy. Nat Rev Cancer 20: 662-680, 2020.
45. Galon J, Costes A, Sanchez-Cabo F, Kirilovsky A, Mlecnik B, Lagorce-Pagès C, Tosolini M, Camus M, Berger A, Wind P, *et al*: Type, density, and location of immune cells within human colorectal tumors predict clinical outcome. Science 313: 1960-1964, 2006.
46. Kenswil KJG, Pisterzi P, Sánchez-Duffhues G, van Dijk C, Lolli A, Knuth C, Vanchin B, Jaramillo AC, Hoogenboezem RM, Sanders MA, *et al*: Endothelium-derived stromal cells contribute to hematopoietic bone marrow niche formation. Cell Stem Cell 28: 653-670.e11, 2021.
47. Valkenburg KC, de Groot AE and Pienta KJ: Targeting the tumour stroma to improve cancer therapy. Nat Rev Clin Oncol 15: 366-381, 2018.
48. Yuan J, Li J, Gao C, Jiang C, Xiang Z and Wu J: Immunotherapies catering to the unmet medical need of cold colorectal cancer. Front Immunol 13: 1022190, 2022.
49. Chen EX, Jonker DJ, Loree JM, He Y, Zhang Y, Hao C, Zeng P, Zhang M, Gao Y, Yang D, *et al*: Effect of combined immune checkpoint inhibition vs best supportive care alone in patients with advanced colorectal cancer: The Canadian cancer trials group CO.26 Study. JAMA Oncol 6: 831-838, 2020.
50. Li H, Wang X, Huang X, He Y, Zhang Y, Hao C, Zeng P, Zhang M, Gao Y, Yang D, *et al*: Circulating glycan monosaccharide composite-based biomarker diagnoses colorectal cancer at early stages and predicts prognosis. Front Oncol 12: 852044, 2022.
51. Lin XT, Wu QN, Qin S, Fan DJ, Lv MY, Chen X, Cai JW, Weng JR, Zou YF, Rong YM and Gao F: Identification of an Autophagy-Related gene signature for the prediction of prognosis in early-stage colorectal cancer. Front Genet 12: 755789, 2021.
52. Ke J, Liu X-H, Jiang X-F, He Z, Xiao J, Zheng B, Chen Y-F, Cai Z-R, Zheng X-B, Zou Y-F, *et al*: Immune-related gene signature in predicting prognosis of early-stage colorectal cancer patients. Eur J Surg Oncol 46: e62-e70, 2020.